



INDONESIAN JOURNAL ON GEOSCIENCE

Geological Agency
Ministry of Energy and Mineral Resources

Journal homepage: <http://ijog.geologi.esdm.go.id>
ISSN 2355-9314, e-ISSN 2355-9306



Optimal Tide Gauge Location for Tsunami Validation in The Lembbeh Island, North Sulawesi

Sesar Prabu Dwi Sriyanto^{1,2}, Ping Astony Angmalisang², and Lusia Manu²

¹Centre of Earthquake and Tsunami, Agency of Meteorology, Climatology and Geophysics,
Jln. Angkasa I No.2 Kemayoran, Jakarta Pusat, Indonesia

²Faculty of Fisheries and Marine Science, Universitas Sam Ratulangi,
Kelurahan Bahu, Kecamatan Malalayang, Kota Manado, Sulawesi Utara 95115, Indonesia

Corresponding author: sesar.sriyanto@gmail.com

Manuscript received: September, 25, 2021; revised: January, 20, 2022;
approved: April, 11, 2022; available online: September, 16, 2022

Abstract - The tsunami early warning system in Bitung does not work optimally, because there is no buoy as a marine equipment for tsunami validation before reaching the coastal area. The lack of buoy can be replaced by placing a tide gauge on the east coast of Lembbeh Island. To determine the optimal tide gauge location, the simple additive weighting (SAW) method was used with three criteria. Those three criteria are the potential of tsunami detection, sufficient evacuation time, and an appropriate site for tide gauge installation. Numerical tsunami modeling is used to calculate the first two criteria. The third criterion is a limiting factor, because the tide gauge can only be installed on the dock. Therefore, there were only five candidate locations on the east coast of Lembbeh, namely Dorbolang, Pancuran, Posokan, Motto, and Lirang. The result, Posokan is the best location for tide gauge placement with a total score of 2.884. Based on the simulation, an additional tide gauge in Posokan can detect tsunami at the average of 11.4 minutes earlier than use only the tide gauge currently available at Bitung port. It means that people on the coast of Bitung have more evacuation time before the tsunami hits the coastal area.

Keywords: tsunami, earthquake, numerical modeling, tide gauge, Lembbeh Island

© IJOG - 2022.

How to cite this article:

Sriyanto, S.P.D., Angmalisang, P.A., and Manu, L., 2022. Optimal Tide Gauge Location for Tsunami Validation in The Lembbeh Island, North Sulawesi. *Indonesian Journal on Geoscience*, 9 (3), p.315-327. DOI: [10.17014/ijog.9.3.315-327](https://doi.org/10.17014/ijog.9.3.315-327)

INTRODUCTION

The Molucca Sea is one of the highest seismicity areas in Indonesia (Figure 1). Based on USGS (United States Geological Survey) (2020), there were fifteen major earthquakes with a magnitude above 7.0 in the range of 1900 - 2019. Furthermore, Sriyanto *et al.* (2019) explains that the dominant earthquake fault mechanism in this area is vertical deformation. This condition potentially causes a tsunamigenic earthquake in the future. Moreover, in the last ten years, three tsunamigenic earth-

quakes had happened on November 15th 2014, July 7th 2019, and November 15th 2019. According to BMKG (Agency of Meteorology, Climatology, and Geophysics) (2019), those three earthquakes have a similar magnitude and source mechanism.

This condition is risky for Molucca Sea coastal community. Bitung City is one of the most dangerous areas, because it is the most populated area in the Molucca Sea coastal zone and has become the second-largest city in the North Sulawesi Province. Morphologically, Bitung located in the flat coastal area, which is vulnerable to tsunami penetration

inland (Yudhicara, 2012). Furthermore, Bitung has an international harbour as the main transportation route in the eastern part of Indonesia. The Indonesian government has designated Bitung as a special economic zone through government regulations number 32 of 2014. Therefore, they need to mitigate tsunami impacts both structurally and culturally.

One of the structural mitigation efforts is strengthening the tsunami early warning system. The Indonesia Tsunami Early Warning System (Ina-TEWS) was inaugurated on November 11th 2008 (UNDRR and UNESCO-IOC, 2019). The tsunami modeling process in the Ina-TEWS triggered by major earthquake parameter as an input. If the modeling result shows that an earthquake could generate a tsunami, the warning message that contains the affected area and its hazard level should be disseminated to the community. Then, the sea level measurement system is monitored to know the certainty of the tsunami. Two types of sea level measurement systems used in tsunami early warning systems are buoy installed offshore and tide gauge installed onshore. After this marine equipment detects a tsunami, people who are still potentially affected should be warned again to evacuate immediately (UNDRR and UNESCO-IOC, 2019). However, a buoy as the offshore instrument does not exist in the Molucca Sea. It is a drawback of the system, because tsunami cannot be detected before reaching the coastal zone.

In order to overcome the problem, the tsunami early warning system in the Bitung coastal area can be improved by placing a tide gauge on the east coast of Lembbeh Island as a substitute for a buoy. The presence of a tide gauge on the east coast of Lembbeh Island will immediately provide the certainty of a tsunami event before it reaches the coast of Bitung. According to Sriyanto *et al.* (2019), the tsunami arrival time on the east coast of Lembbeh Island is about five minutes earlier than the arrival time in the Bitung coastal area. This time interval is very important for the people in the coastal area of Bitung to save themselves to a higher place so that they do not become victims of the tsunami. Furthermore, a tide gauge is cheaper and easy to maintain than a buoy (Bressan *et al.*, 2013). Cur-

rently, tide gauges also developed to be the main consideration in tsunami early warning, not only used in the validation phase of tsunami arrivals. Placing a tide gauge close to a possible source of tsunami generation can immediately provide a tsunami early warning to coastal communities. This system has been implemented in the Mediterranean Sea with a total of forty-one tide gauges, and can be monitored in real-time via the IDSL (Inexpensive Device for Sea Level Measurement) JRC-EC (Joint Research Centre – The European Commission) website (Annunziato *et al.*, 2016; Husrin *et al.*, 2021). It is also developed in Indonesia by integrating about 216 sea-level observation instruments. If there is a sea-level anomaly regarding a tsunami event, a system called InaTNT (Indonesian Tsunami Nontectonic) can provide tsunami warning information without analyzing a prior generator event such as earthquakes, landslides, volcanic activity, and meteor falls (Karyono *et al.*, 2019; Annunziato *et al.*, 2019). Therefore, the optimal location of the tide gauge was analyzed on the east coast of Lembbeh Island, so that the people in the coastal area of Bitung have enough time for evacuating before a tsunami happens.

METHODS AND MATERIALS

Lee *et al.* (2020) explained that the high tsunami detection potential, maximum evacuation time, and the proper site for tsunami observation instrument installation are the criteria for determining the best location for the tsunami observation instrument. The third criteria can become the limitation in finding the optimal location for placing the tide gauge on the east coast of Lembbeh Island, because tide gauges can only be installed on beaches with a dock. On the east coast of Lembbeh, there are only five coastal dock locations, namely Dorbolang, Pancuran, Posokan, Motto, and Lirang. The potential of tsunami detection is measured from the certainty of tsunami detection at each location, while the tsunami arrival time is to calculate the maximum evacuation time.

The simple additive weighting (SAW) method was used for tide gauge location selection, which

is also widely used for decision making from multicriteria problems. The total score of each alternative option (V_i) is calculated from the rating criteria (r_{ij}) and its weighted value (w_j):

$$V_i = \sum_{j=1}^n w_j r_{ij} \quad \dots\dots\dots(1)$$

where i and j are the alternative option index and criteria index, respectively.

In this study, the placement location candidate was used as the alternative option, while the three optimal location criteria from Lee *et al.* (2020) were as the criteria. The three criteria have the same effect in determining the optimal tide gauge location, so each of them has a weight value of 1.0. Each alternative has several data for one criterion, so the rating criteria are calculated from the average of all data according to the following formula:

$$r_{ij} = \frac{\sum_{k=1}^n r_{ij}^k}{n} \quad \dots\dots\dots(2)$$

where:

r_{ij}^k is the rating of k -th data of j -th criteria at i -th candidate location, while n and k are the numbers of data and data index, respectively.

The rating of the first criteria are determined from the certainty of tsunami detection at each location. If a tsunami can be detected, the candidate location rating is 1.0. However, the criterion is 0 if the tsunami time-series data cannot be detected using the detection algorithm. The detection algorithm calculates the tsunami signal presence in the time-series data after it is filtered from the tidal effect (Mojfeld, 1997). A tsunami can be detected if the filtered time-series data exceeds the threshold of the tsunami detection algorithm. The threshold value used is 30 cm.

For the second criteria, tsunami arrival time is used for counting the rating of each candidate location. The earliest tsunami arrival time is the best value, so the rating value is calculated based on the following equation (Setyawan *et al.*, 2017):

$$r_{i2}^k = \frac{\min(t_k)}{t_{i,k}} \quad \dots\dots\dots(3)$$

where:

r_{i2}^k is the second criteria rating of k -th data at i -th candidate location,

$t_{i,k}$ is the value of the tsunami arrival time from the k -th data recorded at the i -th candidate location,

$\min(t_k)$ is the minimum value of the tsunami arrival time from the k -th data.

In contrast, the existence of a dock at each location caused the third criterion rating value to be set at 1.0.

Due to limited tsunami events in this area and limited tsunami observation data on the east coast of Lembah Island, the arrival time and time-series tsunami height data at each candidate location are obtained from tsunami propagation modeling. Lee *et al.* (2020) and Meza *et al.* (2020) also use numerical tsunami modeling to determine the best location of tsunami detection instruments in Korea and Chile, respectively. Based on USGS (2020), major earthquakes with a magnitude above 7.0 concentrate in the middle of the Molucca Sea. It is related to the tectonic structure of the Talaud-Mayu Ridge, which has a southwest - northeast direction (Zhang *et al.*, 2017). Therefore, the tsunami propagation modeling uses the earthquake in the middle of the Molucca Sea as a tsunami generator source scenario.

To obtain the representation of tsunami characteristics in this area, nine scenarios were used with variations in location and magnitude. The source location varies in three points are southwest section with the geographical coordinates 0.493°N - 125.805°E, the middle section in coordinate 1.483°N - 126.376°E, and the northwest section with the coordinate 2.305°N - 126.760°E. Meanwhile, three variations of the earthquake magnitude used are Mw 7.5, Mw 8.0, and Mw 8.5. This magnitude range was chosen based on tsunamigenic earthquake minimum magnitude from BMKG (2012) and Molucca Sea maximum

magnitude estimation by Raharjo *et al.* (2013). For other parameter, each scenario used the same value. The strike and dip parameter use the average value from the historical data, while the rake angle use 90° as the worst case scenario tsunami generated (Titov *et al.*, 1999, in Necmioğlu and Özel, 2014). Also, the focal depth uses a shallow earthquake with a value of 10 km, because it can trigger a tsunami with the maximum amplitude. Figure 1 shows the location of the earthquake epicentre scenario for tsunami modeling and the earthquake epicentre with a magnitude of > 7.0 that had occurred in the Molucca Sea for the period of 1900–2019 (USGS, 2020).

Furthermore, the input for tsunami modeling needs the fault plane size. The length (L), width (W), and slip deformation derived from the magnitude value use the empirical equation known as Scaling Law. Based on the validation of 2014 Molucca Sea tsunami modeling with tide gauge observation by Gusman *et al.* (2017), the Scaling Law equation from Blaser *et al.* (2010) showed

a strong correlation with the observation results. The following equation is the equation of Blaser *et al.* (2010) for the thrust fault types:

$$\log L = 0,57 M_w - 2,37 \dots\dots\dots(4)$$

$$\log W = 0,46 M_w - 1,86 \dots\dots\dots(5)$$

where M_w is the moment magnitude. Meanwhile, slip deformation (D) was obtained from the equation by Aki (1966) and the empirical equation of the relationship between moment magnitude and seismic moment (Hanks and Kanamori, 1979):

$$D = \frac{M_o}{\mu LW} \dots\dots\dots(6)$$

$$\log M_o = 1,5 M_w + 9,05 \dots\dots\dots(7)$$

where:

M_o is seismic moment in units of Nm and μ is the rigidity value of 4×10^{10} N/m².

All parameters of each scenario are showed in Table 1.

Tsunami propagation simulation used the MOST (Method of Splitting Tsunami) model, which run using ComMIT (Community Model Interface for Tsunami) software (Titov *et al.*, 2011). The computation of tsunami propagation in the deep sea used the linear wave theory, while the shallow water theorem was used for the propagation in the shallow water. The sea surface fluctuation at each grid point in the modeling area was calculated numerically using a leap-frog scheme. The elevation data used in ComMIT consist of ETOPO1 bathymetry and SRTM (Shuttle Radar Topography Mission) topography data. Bathymetric data has a resolution of up to 1 arc minute, while topographic data resolution is 90 m.

The nesting grid method was also used in the ComMIT modeling process to obtain high resolution results in the researched area. In the nesting grid method, the modeling area was divided into three domains presented as maps (Figure 2) for

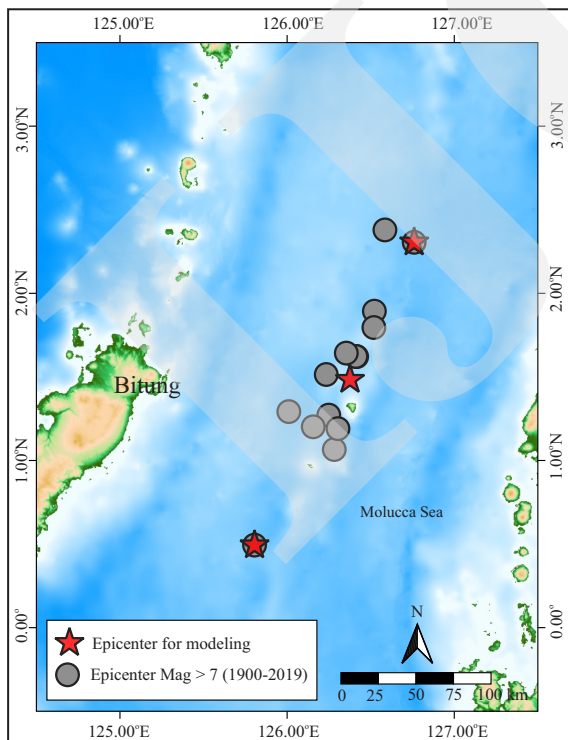


Figure 1. Location of the earthquake epicentre scenario for tsunami modeling and the earthquake epicentre with a magnitude of ≥ 7.0 that had occurred in the Molucca Sea for the period of 1900–2019 (USGS, 2020).

Table 1. Earthquake Source Scenarios for Tsunami Propagation Simulation

Name	Lat (°)	Long (°)	Mag	L (km)	W (km)	Strike (°)	Dip (°)	Rake (°)	Slip (m)	Depth (km)
Scenario 1	0.493	125.805	7.5	80.35	38.90	27.8	55	90	1.60	10
Scenario 2	0.493	125.805	8.0	154.88	66.07	27.8	55	90	2.74	10
Scenario 3	0.493	125.805	8.5	298.54	112.20	27.8	55	90	4.71	10
Scenario 4	1.483	126.376	7.5	80.35	38.90	27.8	55	90	1.60	10
Scenario 5	1.483	126.376	8.0	154.88	66.07	27.8	55	90	2.74	10
Scenario 6	1.483	126.376	8.5	298.54	112.20	27.8	55	90	4.71	10
Scenario 7	2.305	126.760	7.5	80.35	38.90	27.8	55	90	1.60	10
Scenario 8	2.305	126.760	8.0	154.88	66.07	27.8	55	90	2.74	10
Scenario 9	2.305	126.760	8.5	298.54	112.20	27.8	55	90	4.71	10

tsunami modeling. Domain A covers the tsunami source area to the coastal (Figure 2a), domain B is the transitional domain (Figure 2b), and domain C only focuses on the region of interest. Two areas of domain C were used to get the high resolution for each candidate location. Domain C1 is located in northern Lembah (Figure 2c), while domain C2 covers the southern Lembah area (Figure 2d).

One of the outputs of this modeling is the sea surface fluctuation at each point of the modeling area. Sea surface fluctuations in each five candidate locations were analyzed to obtain the certainty of tsunami detection and arrival time. In addition, the analysis of sea surface fluctuation was also carried out at five locations along the coast of Bitung as a comparison. These locations are Manembo-nembo, Girian Bawah, Paceda,

Bitung Timur, and Aertembaga Satu. The ten locations, where sea surface fluctuation were analyzed, are known as virtual tide gauge locations. The distribution of the virtual tide gauges can be seen in Figure 2.

RESULT AND DISCUSSION

Modeling results show that the parameters of the earthquake scenario affect the initial sea surface displacement. The earthquake magnitude strongly affects the area of the initial sea surface displacement. An increase in earthquake magnitude led to the larger lifted water column, as can be seen in Figure 3. Figures 3c, 3f, and 3i show that an earthquake with a magnitude of 8.5 can

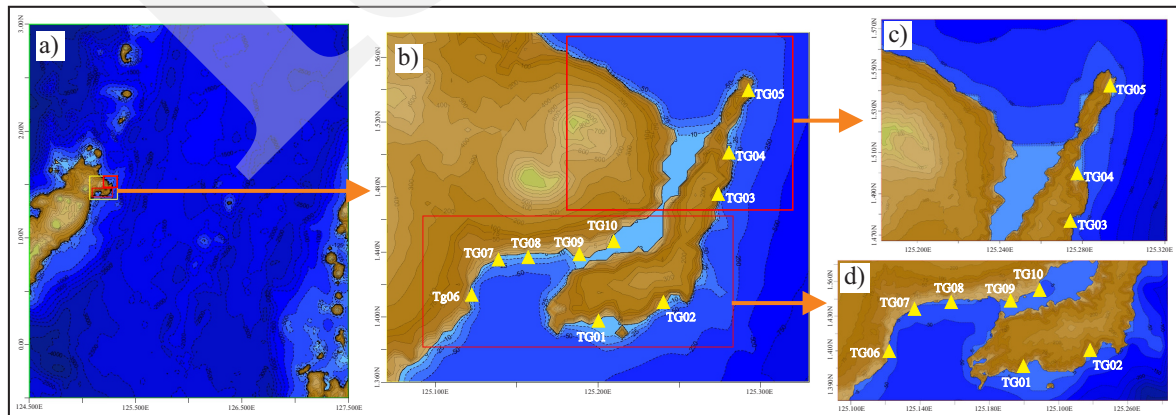


Figure 2. Map of the domain area for tsunami modeling and distribution of virtual tide gauge locations. a) Domain A, b) domain B, c) domain C1, and d) domain C2. TG09 location denotes the current available tide gauge in port of Bitung.

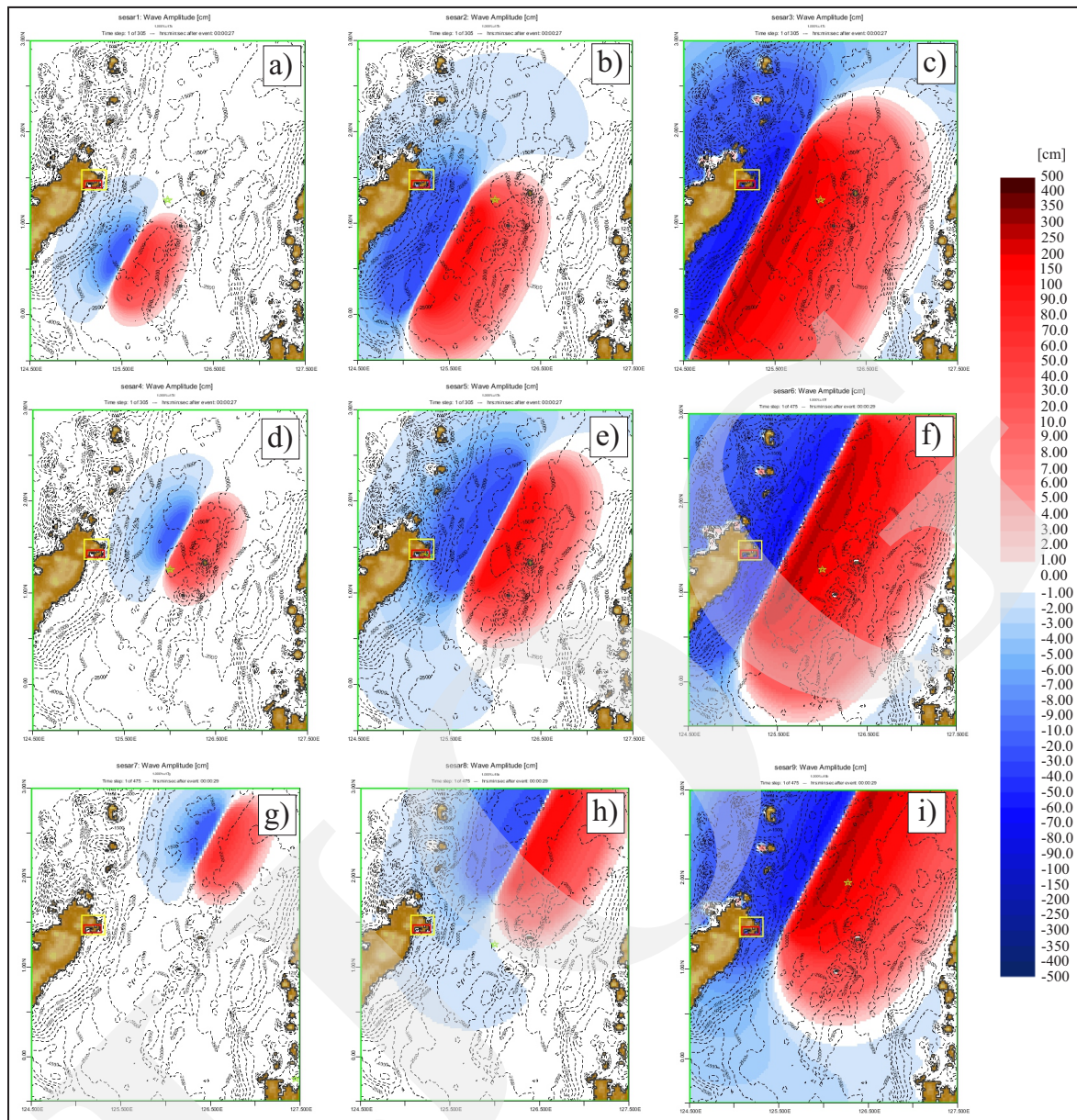


Figure 3. Initial sea surface displacement generated by a) Scenario 1, b) Scenario 2, c) Scenario 3, d) Scenario 4, e) Scenario 5, f) Scenario 6, g) Scenario 7, h) Scenario 8, and i) Scenario 9.

generate sea surface displacement in almost all the Molucca Sea waters. Meanwhile, a smaller magnitude scenario triggers a narrower initial disturbance area. Each scenario generates a similar initial sea surface displacement pattern. The northwest side of the fault always decreases sea surface first, while the southeast side influences the source rises. It is because the earthquake source mechanism uses the same strike, dip, and rake angles. A strike value of 27.8° and a rake angle of 90° produces a sea surface increase

extending from the northeast–southwest with a sea surface decrease in the northwest side (perpendicular to the strike direction).

Figure 4 shows the time series of sea-level fluctuations until two hours after the earthquake origin time at each prospective tide gauge location in each scenario. This data indicates sea-level change due to tsunami by ignoring the tidal factor. To determine the certainty of tsunami detectable by the algorithm, it is only necessary to see whether the maximum tsunami height exceeds the

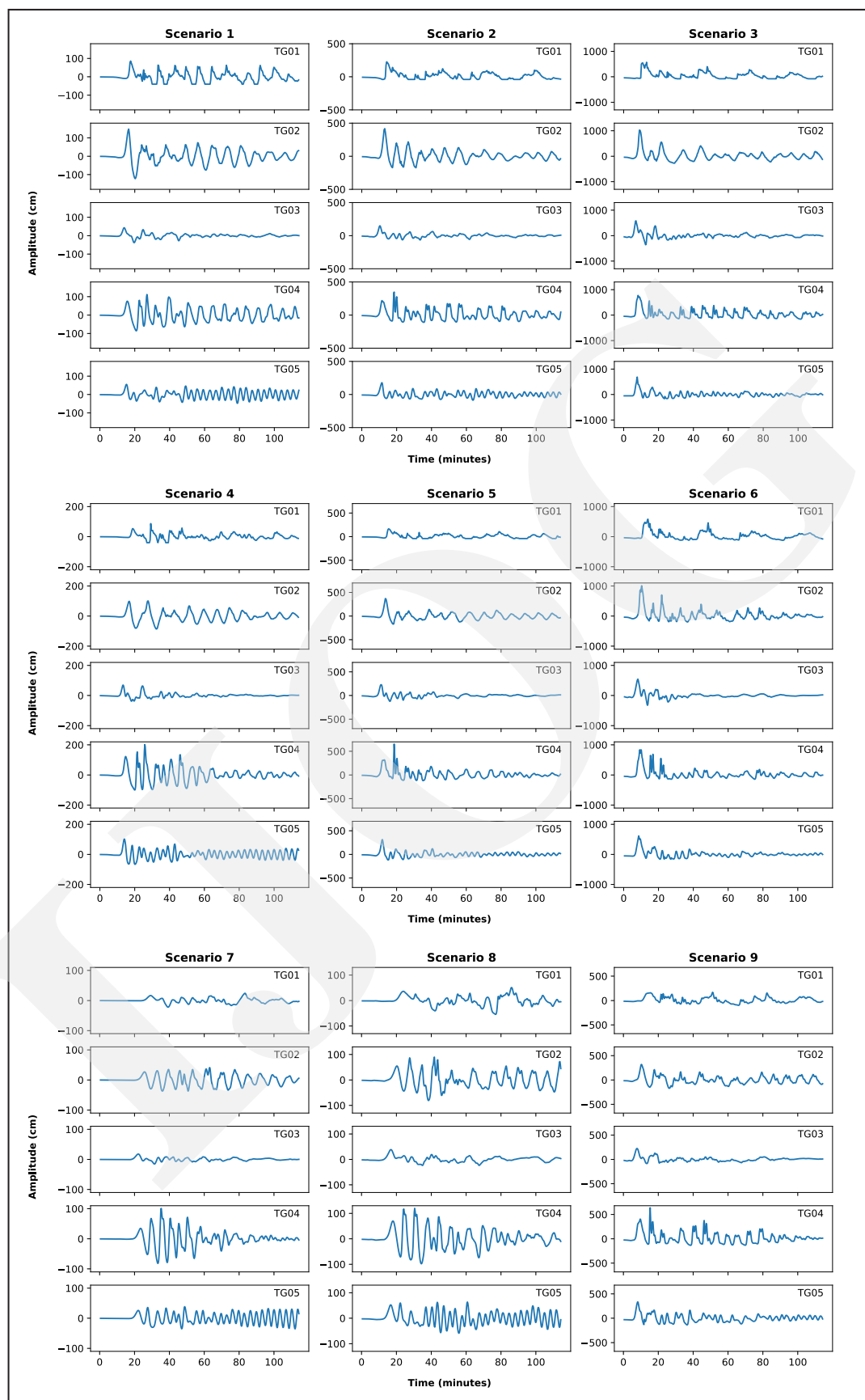


Figure 4. Modeled sea surface fluctuation at five tide gauge candidate locations for nine tsunami scenarios.

defined threshold or not. In general, the highest tsunami height is in the TG02 location, while the lowest is in the TG03 location. The beach curvature influences the tsunami height in each candidate location. The increasing curvature of the coast causes the tsunami to be higher. The tsunamis at TG04 and TG05, located in the bay, are still high. However, the flatter shape of the coast at TG01 and TG03 causes the tsunami to be lower. Figure 5 shows the satellite imagery from google earth of each candidate location. The bay-shaped coast causes wave reflection and refraction, resulting in interference or wave reinforcement in these waters. Yudhicara *et al.* (2014) also explains that the tsunami height tends to be higher in the bay-shaped waters than the flat-shaped ones, because there is a mass of water that has accumulated into these waters. Moreover, the tsunami source location also affects the tsunami

height. Tsunami waves attenuate as the tsunami propagation distance increases. The southwestern source section is closer to TG02 than TG04, and causes tsunamis at TG02 to be higher than those in TG04. It has also occurred to TG04, which is closer to the northeast source section. Figure 6 shows the maximum tsunami height from each scenario at each candidate location.

Almost the maximum tsunami height at each location exceeds the threshold of tsunami detection. However, two candidate locations record tsunami below the threshold value. The tsunami propagation modeling from scenario 7 hits TG01 and TG03 with a maximum amplitude of 24.06 and 17.73 cm, respectively. It could not be detected by the algorithm because of the maximum amplitude below 30 cm as the threshold value. It causes the first criteria rating of TG01 and TG03 to be 0.889. Meanwhile, the other candidate loca-



Figure 5. Satellite imagery from google earth of a) TG01, b) TG02, c) TG03, d) TG04, and e) TG05.

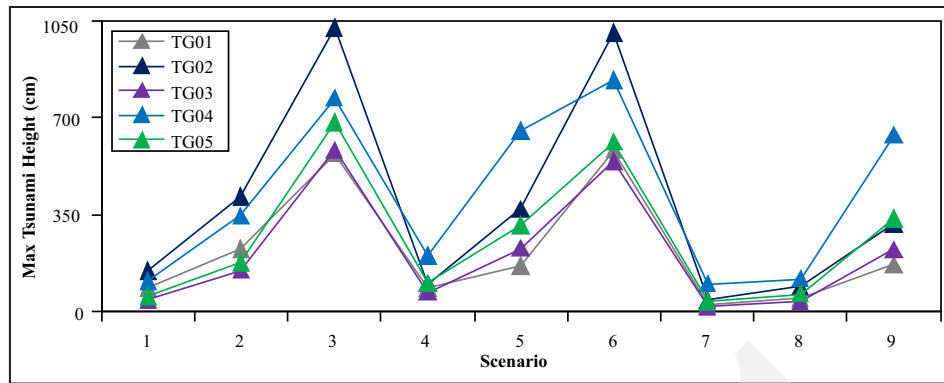


Figure 6. Maximum tsunami height from each scenario at each candidate location.

tions get the maximum first criteria rating with a value of 1.0.

For the second criteria, TG03 always gets the highest score except in scenario 8. The tsunami propagation time strongly depends on earthquake magnitude and bathymetry. As can be seen in Figure 3, earthquake magnitude influences the initial sea surface displacement area. If the sea surface displacement area becomes wider, the tsunami arrival time on the coast will be faster. Although the source is in the same location, the tsunami can reach the coastal area more quickly due to the larger earthquake magnitude, as shown in Figure 7. The contour of bathymetry affects the tsunami propagation too. The gentle bathymetric contours on the coastal area reduce the speed of tsunami propagation. Therefore, the tsunami is always slower to arrive at TG02 and TG01 than at TG03-TG05 in all scenarios. Figure 8 shows the animation of the tsunami propagation model in the case of scenario 2. The tsunami has reached TG03 eight minutes after the earthquake, then

it arrives in TG04 and TG05 in the 9th minute. Afterward, the tsunami strikes TG02 in the 10th minute and TG01 in the 13th minute.

The second criteria is the dominant factor for the tsunami observation instrument location. The tsunami arrival time in each candidate location is significantly different. It greatly determines the availability of evacuation time for people on the Bitung Coast. Meanwhile, the certainty of tsunami detection does not have a strong influence, because almost all tsunami scenarios can be detected well. Although there is an undetected tsunami scenario, the tsunami propagation model is not expected to have a strong impact on the Bitung Coast, because the tsunami height on the Bitung Coast is mostly smaller than the tsunami height on the east coast of Lembeh Island. The results of the calculation of all criteria, the location of TG03 is the best location for the tide gauge placement with the total score of 2.884. TG03 has the first criterion rating of 0.889, the second criterion rating of 0.995, and the third criterion

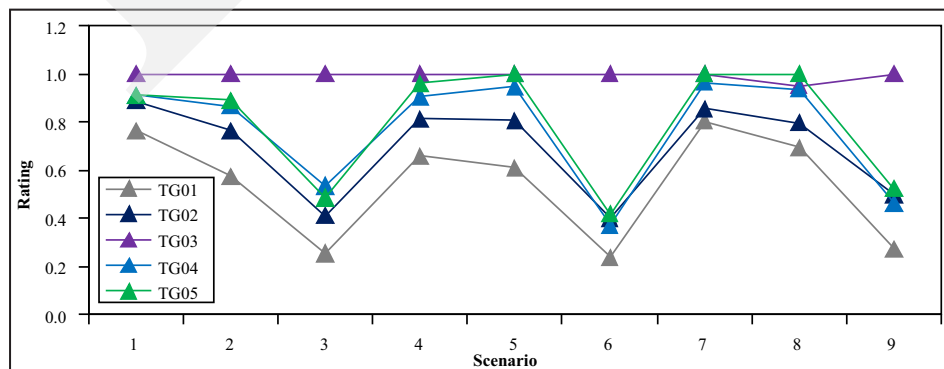


Figure 7. Score of the second criteria from each scenario at each candidate location.

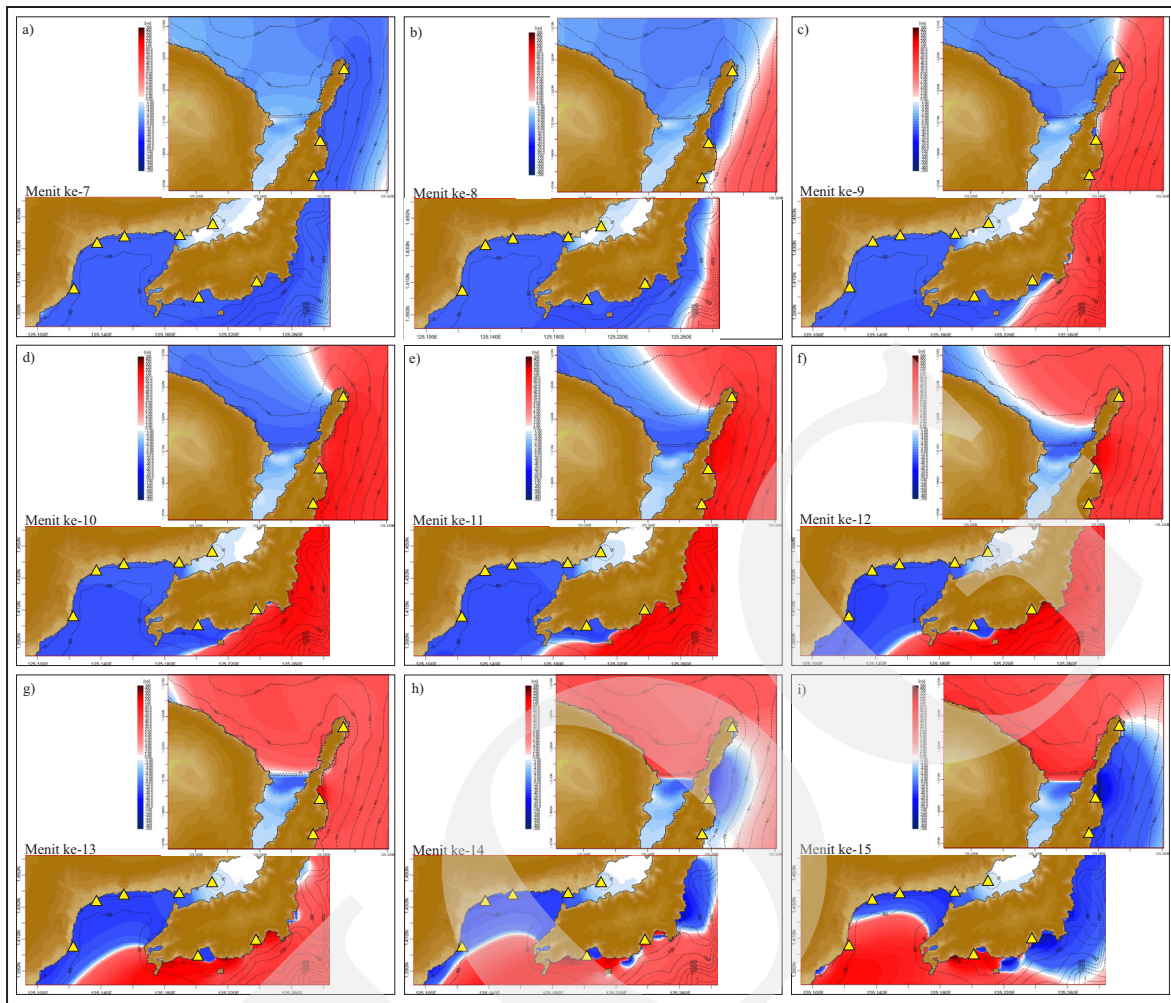


Figure 8. Tsunami propagation model in case of scenario 2 in a) 7th minute, b) 8th minute, c) 9th minute, d) 10th minute, e) 11th minute, f) 12th minute, g) 13th minute, h) 14th minute, and i) 15th minute.

rating of 1.000. The total score of all candidate locations is shown in Table 2.

Based on the tsunami simulation, TG03 can detect tsunami earlier than using only the tide gauge currently available at Bitung Port. TG09 represents the port of Bitung in this simulation.

Tabel 2. Total Score of All Candidate Locations

Code	Rating Criteria 1	Rating Criteria 2	Rating Criteria 3	Total Score
TG01	0.889	0.541	1.000	2.430
TG02	1.000	0.692	1.000	2.692
TG03	0.889	0.995	1.000	2.884
TG04	1.000	0.767	1.000	2.767
TG05	1.000	0.798	1.000	2.798

TG03, located in Posokan Village, records tsunami in the range of 9.4–12.9 minutes and an average of 11.4 minutes before tsunami strike Bitung Port. As mentioned in Table 3, the tsunami arrival time at TG03 was earlier in the range of 4.56–23.04 minutes compared to the virtual tide gauge located on the coast of Bitung (TG06–TG10). This difference in the tsunami arrival time can provide additional time for people on the coast of Bitung to immediately evacuate themselves after the tide gauge in Posokan Village detects a tsunami.

These results show the efforts for providing more evacuation time for the people of Bitung by adding the tide gauge device to validate the tsunami earlier before it arrives on the coast of Bitung. However, it needs to be considered to

Table 3. Arrival Time Difference between TG03 and Virtual Tide Gauge Located on The Coast of Bitung

Scenario	Difference of Arrival Time (minutes)				
	TG06-TG03	TG07-TG03	TG08-TG03	TG09-TG03	TG10-TG03
Scenario 1	4.56	5.68	6.05	9.41	19.49
Scenario 2	6.13	7.25	7.63	11.73	20.32
Scenario 3	7.68	8.80	9.17	12.91	20.00
Scenario 4	7.15	8.27	8.64	11.63	21.71
Scenario 5	6.16	7.28	8.03	11.39	21.09
Scenario 6	8.16	9.12	9.60	12.72	20.40
Scenario 7	7.44	7.68	8.16	12.00	23.04
Scenario 8	7.44	8.16	8.40	10.80	22.32
Scenario 9	8.64	9.60	9.84	10.32	22.32

analyze the tide gauge potential locations at the small islands in the centre of the Molucca Sea, namely Mayu and Tifore Islands. These islands are closer to the earthquake sources, but it should be noticed that the telecommunication factor also has an important role. The telecommunication network is not yet available in all regions, especially on the small islands. It could be delaying the real-time data transmission from the tide gauge site to the data server. For further study, it is necessary to take into account the telecommunication aspect of tide gauge data transfer and the closest possible location to the earthquake sources, so that it can detect a tsunami as soon as possible (Annunziato *et al.*, 2019).

CONCLUSIONS

Posokan is the best location for tide gauge placement with the total score of 2.884. In detail, the rating of tsunami detection potential, sufficient time evacuation, and appropriate site for tide gauge installation criteria are 0.889, 0.995, and 1.0, respectively. Based on numerical tsunami modeling, the addition of a tide gauge in Posokan can detect tsunami in an average of 11.4 minutes earlier than only using the existing tide gauge in Bitung Port. The tsunami reached the coast of Bitung in a range of 4.56–23.04 minutes after arriving at Posokan, so the people of Bitung could use that time to evacuate immediately.

ACKNOWLEDGMENTS

The authors would like to appreciate Manado Geophysical Station and Sam Ratulangi University for the support in writing this paper. They also thank reviewers for their suggestions and valuable comments.

REFERENCES

- Aki, K., 1966. Generation and Propagation of G Waves from the Niigata Earthquake of June 16, 1964: Part 2. Estimation of Earthquake Moment, Released Energy, and Stress-strain Drop from G Waves Spectrum. *Bulletin of the Earthquake Research Institute*, 44, p.73-88.
- Annunziato, A., Galliano, D., and Bonaita, M., 2016. IDSL Sea Level Measurement Devices. *Technical Report JRC-EC*. DOI: 10.2788/470647.
- Annunziato, A., Prasetya, G., and Husrin, S., 2019. Anak Krakatau Volcano Emergency Tsunami Early Warning System. *Science of Tsunami Hazards*, 38 (2), p68-95.
- Blaser, L., Krüger, F., Ohrnberger, M., and Scherbaum, F., 2010. Scaling Relations of Earthquake Source Parameter Estimates with Special Focus on Subduction Environment. *Bulletin of the Seismological Society of America*, 100 (6), p2914-2926. DOI: 10.1785/0120100111.

- BMKG, 2019. *Earthquake Catalogue*. [Http://repogempa.bmkg.go.id/repo_new/](http://repogempa.bmkg.go.id/repo_new/) [20th December 2019].
- BMKG, 2012. *Pedoman Pelayanan Peringatan Dini Tsunami*. Badan Meteorologi Klimatologi dan Geofisika. BMKG, Jakarta, 137 pp.
- Bressan, L., Zaniboni, F., and Tinti, S., 2013. Calibration of a Real-time Tsunami Detection Algorithm for Sites with No Instrumental Tsunami Records: Application to Coastal Tide-gauge Stations in Eastern Sicily, Italy. *Natural Hazards and Earth System Science*, 13, p.3129-3144. DOI: 10.5194/nhess-13-3129-2013.
- Gusman, A.R., Nugraha, A.D., and Shiddiqia, H.A., 2017. Hypocenter Relocations and Tsunami Simulation for the 15 November 2014 Northern Molucca Sea Earthquake in Indonesia. *Jurnal Geofisika*, 15 (1), p.1-9.
- Hanks, T.C. and Kanamori, H., 1979. A Moment Magnitude Scale. *Journal of Geophysical Research*, 84, p.2348-2350. DOI: 10.1029/JB084iB05p02348.
- Husrin, S., Novianto, D., Bramawanto, R., Setiawan, A., Nugroho, D., Permana, S.M., Sufyan, A., Sarnandal, Sianturi, D.S.A., Mulyadi, U., Daniel, D., Suhelmi, I.R., Purnama, M.S.B., 2021. Analisa Kinerja IDSL/PUMMA untuk Peringatan Dini Tsunami di Pangandaran. *Jurnal Kelautan Nasional*, 16 (2), p87-98.
- Karyono, Arifin, J., Daryono, Weniza, Triyono, R., and Sadly, M., 2019. Development of New InaTEWS SOP to include Non-Tectonic Tsunami Warning System. *Presented at International Symposium on the Lesson Learnt from the 2018 Tsunamis in Palu and Sunda Strait*. [Http://www.ioc-tsunami.org/index.php?option=com_oe&task=viewDocumentRecord&docID=26428](http://www.ioc-tsunami.org/index.php?option=com_oe&task=viewDocumentRecord&docID=26428) [21st December 2021].
- Lee, E., Jung, T., and Shin, S., 2020. Numerical and Probabilistic Study on the Optimal Region for Tsunami Detection Instrument Deployment in the Eastern Sea of Korea. *Applied Science*, 10, 6071. DOI: 10.3390/app10176071.
- Meza, J., Catalán, P.A., and Tsushima, H., 2020. A Multiple-Parameter Methodology for Placement of Tsunami Sensor Networks. *Pure and Applied Geophysics*, 177, p.1451-1470. DOI: 10.1007/s00024-019-02381-3.
- Mojfeld, H.O., 1997. *Tsunami Detection Algorithm*. https://nctr.pmel.noaa.gov/tda_documentation.html [27th March 2020].
- Necmioğlu, O. and Özel, N.M., 2014. An Earthquake Source Sensitivity Analysis for Tsunami Propagation in the Eastern Mediterranean. *Oceanography*, 27 (2), p.76-85. DOI: 10.5670/oceanog.2014.42.
- Raharjo, S.S., Mamuaya, G.E., and Lumingas, L.J.L., 2013. Mapping of Tsunami Prone Areas in Coastal Region of Kema, North Sulawesi. *Aquatic Science & Management*, 1, p.40-47.
- Setyawan, A., Arini, F.Y., and Akhlis, I., 2017. Comparative Analysis of Simple Additive Weighting Method and Weighted Product Method to New Employee Recruitment Decision Support System (DSS) at PT. Warta Media Nusantara. *Scientific Journal of Informatics*, 4 (1), p.34-42.
- Sriyanto, S.P.D., Nurfitriani, Zulkifli, M., and Wibowo, S.N.E., 2019. Pemodelan Inundasi dan Waktu Tiba Tsunami di Kota Bitung, Sulawesi Utara Berdasarkan Skenario Gempabumi Laut Maluku. *Geomatika*, 25 (1), p.47-54. DOI: 10.24895/JIG.2019.25-1.959.
- Titov, V.V., Mojfeld, H.O., Gonzalez, F.I., and Newman, J.C., 1999. Offshore Forecasting of Hawaiian Tsunamis Generated in Alaskan- Aleutian Subduction Zone. *NOAA Technical Memorandum ERL PMEL-114, Pacific Marine Environmental Laboratory, USA*, 26pp., [Http://www.pmel.noaa.gov/pubs/PDF/tito2049/tito2049.pdf](http://www.pmel.noaa.gov/pubs/PDF/tito2049/tito2049.pdf) [27 March 2020].
- Titov, V.V., Moore, C.W., Greenslade, D.J.M., Pattiaratchi, C., Badal, R., Synolakis, C.E., and Kânoğlu, U., 2011. A New Tool for Inundation Modeling: Community Modeling Interface for Tsunamis (ComMIT). *Pure and Applied Geophysics*, 168, p.2121-2131. DOI: 10.1007/s00024-011-0292-4.
- UNDRR and UNESCO-IOC, 2019. *Limitations and Challenges of Early Warning Systems: A Case Study of the Palu-Donggala Tsunami*.

- United Nations Office for Disaster Risk Reduction (UNDRR), Jakarta, 66 pp.
- USGS, 2020. *Earthquake Catalog*. <https://earthquake.usgs.gov/earthquakes/search/> [12 November 2020].
- Yudhicara, 2012. Tsunami Characteristics along The Coast of Biak Island based on the 1996 Biak Tsunami Traces. *Jurnal Geologi Indonesia (Indonesian Journal on Geoscience)*, 7 (1), p.55-66.
- Yudhicara, Robiana, R., and Priambodo, I.C., 2014. The Influence of Coastal Conditions to Tsunami Inundation of Bima Bay, West Nusa Tenggara. *Bulletin of the Marine Geology*, 29 (1), p.29-42.
- Zhang, Q., Guo, F., Zhao, L., and Wu, Y., 2017. Geodynamics of Divergent Double Subduction: 3-D Numerical Modeling of a Cenozoic Example in the Molucca Sea Region, Indonesia. *Journal of Geophysical Research: Solid Earth*, 122, p.3977-3998. DOI: 10.1002/2017JB013991.